Nanoimprinted superlattice metallic photonic crystal as ultra-selective solar absorber

V. Rinnerbauer,[1,*] E. Lausecker,[1] F. Schäffler,[1] P. Reininger,[2] G. Strasser,[2] R. D. Geil,[3] J. D. Joannopoulos,[4] M. Soljačić,[4] and I. Celanovic[4]

[1]*Insitute of Semiconductor and Solid State Physics, Johannes Kepler University, Linz, 4040, Austria*

[2]*Institute for Solid State Electronics, Technical University, Vienna, 1040, Austria*

[3]*Department of Applied Physical Sciences, University of North Carolina, Chapel Hill, North Carolina, 27599, USA*

[4]*Institute of Soldier Nanotechnologies, Massachusetts Institute of Technology, Cambridge, Massachusetts, 02139, USA*

**Corresponding author: veronika.rinnerbauer@jku.at*

A two-dimensional superlattice metallic photonic crystal (PhC) and its fabrication by nanoimprint lithography on tantalum substrates are presented. The superior tailoring capacity of the superlattice PhC geometry is used to achieve spectrally selective solar absorbtion optimized for high temperature and high efficiency solar energy conversion applications. The scalable fabrication route by nanoimprint lithography allows for a high-throughput and high-resolution replication of this complex pattern over large areas. Despite the high fill factor, the pattern of polygonal cavities is accurately replicated into a resist that hardens under ultra-violet radiation over an area of 10 mm². In this way, cavities of 905 nm and 340 nm width are achieved with a period of 1 µm. After pattern transfer into tantalum via a deep reactive ion etching process, the achieved cavities are 2.2 µm deep, separated by 85-95 nm wide ridges with vertical sidewalls. The room temperature reflectance spectra of the fabricated samples show excellent agreement with simulated results, with a high spectral absorptance approaching blackbody absorption in the range from 300-1900 nm, and a steep cut-off. The calculated solar absorptivity of this superlattice PhC is 96% and its thermal transfer efficiency is 82.8% at an operating temperature of 1500 K and an irradiance of 1000 kW/m2.

OCIS codes: *(160.5298) Photonic crystals; (220.4241) Nanostructure fabrication; (350.6050) Solar energy.*

http://dx.doi.org/10.1364/optica.99.099999

In the last decade, the field of high-temperature photonics is growing rapidly due to an increased scientific interest as well as emerging applications, especially in the field of energy conversion. In this field, the challenges photonic components have to meet are high temperature stability over long lifetimes, high tailoring capacity of the optical properties, and economic fabrication over large areas. In this study, a superlattice PhC consisting of polygonal cavities gave superior control over the spectral properties to achieve a highly selective solar absorber with low thermal emission for high temperature energy conversion applications. For the first time, a metallic superlattice PhC absorber was fabricated by nanoimprint lithography (NIL) as a high-throughput, high-resolution technique paving the way for complex high-temperature photonic components on a large scale.

Selective thermal absorbers and emitters are critical components for high temperature and high-efficiency energy conversion applications, such as thermophotovoltaics (TPV), solar TPV, and solar thermal systems. TPV is a thermal-to-electrical energy conversion scheme where thermal emission from a hot radiation source (emitter) drives a suitable photovoltaic cell, promising low maintenance, scalability, high power densities as well as flexibility regarding the employed fuel. In solar TPV (STPV), the irradiation from the sun on an absorber is converted into narrow-band thermal radiation on the emitter side.[1] To reach the high efficiencies predicted by theoretical studies[2-4] it is crucial to (1) reach high operating temperatures (>1000 K) and (2) to employ spectrally selective components with low thermal emissivity, in order to reduce losses due to waste heat by re-radiation. In the past, PhCs from refractory metals have been used for spectrally selective solar absorbers and thermal emitters.[5-10] Refractory metals are ideally suited to achieve thermal stability over long lifetimes due to their high melting point and low vapor pressure. Thermal stability of the nanostructured PhCs is critical[11] and it has been demonstrated that 2D and 3D PhCs with critical dimensions below 100 nm are stable at temperatures exceeding 1200 K by using surface protection coatings of hafnium oxide (HfO_2).[12-14] 2D PhCs can be used to achieve spectral selectivity, which is critical for thermal absorbers and emitters in STPV systems.[15-17] A superlattice PhC however allows for even greater design flexibility to tailor the properties to specific needs. A selective solar absorber based on a 2D superlattice PhC with high fill factor, consisting of two polygonal cavities per unit cell, has been proposed which exhibits spectral absorptance approaching that of a blackbody over most of the solar spectrum.[18] In this design, the contribution from electromagnetic modes of both cavities enhances the intrinsic absorptivity in a broad spectral range, which can be tailored by changing the geometrical parameters of the cavities. Simultaneously, the absorptivity has a steep cut-off and is low at longer wavelengths, fulfilling the critical requirement for low thermal losses.

In the past, 2D PhCs for selective emitters and absorbers were fabricated on tungsten (W) and tantalum (Ta) substrates as well as TaW alloys[19-21] using electron-beam lithography (EBL)[7] or interference lithography (IL).[5,19-21] The first method is expensive and limited in throughput and area; the second one is capable of exposing large areas, but is inherently limited to simple patterns such as square lattices of cylindrical cavities. In this study, nanoimprint lithography (NIL) was used as a high-throughput, high-resolution nanostructuring technique that allows for complex and dense patterns to be replicated from a master stamp with high reproducibility and uniformity over large areas.[22-24] We employed UV-NIL for which the surface pattern of a stamp is mechanically pressed into a resist, which is then hardened by exposure to ultraviolet (UV) light through the transparent stamp, before the stamp is released. One advantage over EBL is that one master stamp containing the pattern can be used to structure large areas e.g., by step-and-repeat technique. In contrast to IL any 2D pattern can be replicated**,** and even 3D structures that do not have an undercut. In addition, the size of the patterned area is controlled by the master, which is of particular interest for solar TPV applications, where the area ratio of absorber and emitter can be optimized to achieve highest efficiencies.[2,16,18]

In this study, a 2D superlattice PhC consisting of octagonal and square cavities (see Fig. 1(a)) with a geometry optimized for a solar absorber operating at a high operating temperature (1500 K) and a high incident irradiance (1000 kW/m^2) was fabricated by UV-NIL on polished Ta substrates. The optimized structure had a period a=1.0 µm with narrow ridges between the cavities of 95 nm and 85 nm width, and an etch depth of at least 2 µm in Ta. Despite the high fill factor of almost 80%, which is the ratio of the cavity area to the overall area, the pattern was accurately imprinted over an area of 10mm^2 into the resist, resulting in 200 nm high ridges with an aspect ratio of 2:1 and steep sidewalls. The pattern was then transferred into a silicon dioxide (SiO_2) hard mask using standard semiconductor processes, and finally into the Ta substrate using an optimized gas-chopping deep reactive ion etching process (DRIE, referred to as Bosch process). An additional coating of 40 nm of HfO_2 was used to provide thermal stability as well as increased absorptivity in the visible range.[14,18] The spectral absorptance of the fabricated PhCs was determined from reflectance measurements at room temperature in the range of 0.3 µm to 10 µm using a Fourier-transform infrared spectrometer (FTIR) and a spectrophotometer with an integrating sphere. The measured spectra showed low reflectance approaching zero in the visible range, and high reflection approaching that of flat Ta in the long wavelength range, being in excellent agreement with the simulated results.

Polished, pre-annealed Ta sheets of 500 µm thickness were used as substrates. As a mask for the final deep reactive ion etching (DRIE) of Ta, a layer of 100 nm SiO_2 was deposited on the substrates by plasma-enhanced chemical vapor deposition (PECVD), using 425 sccm SiH_4, 2% N_2 and 710 sccm N_2O at 300°C and a power of 10 W). The superlattice pattern was created by UV-NIL using an EVG620 mask aligner. The stamp was replicated from a NIL template, containing the superlattice PhC pattern etched to a depth of 200 nm into a silicon (Si) substrate (IMS Chips, Germany). Since the Ta substrates were more rigid than the more commonly used Si substrates, a flexible stamp had to be used in order to establish close, uniform contact during nanoimprinting. Therefore, a 150 µm thin glass slide served as stamp backplate. An additional compliant layer of polydimethylsiloxane (PDMS, ~900 µm thick) in the same size as the substrate was placed on top of the flexible stamp during imprinting to ensure uniform contact and to level out any substrate unevenness or stamp deformations[25] (see schematic in Fig. 1(b)).

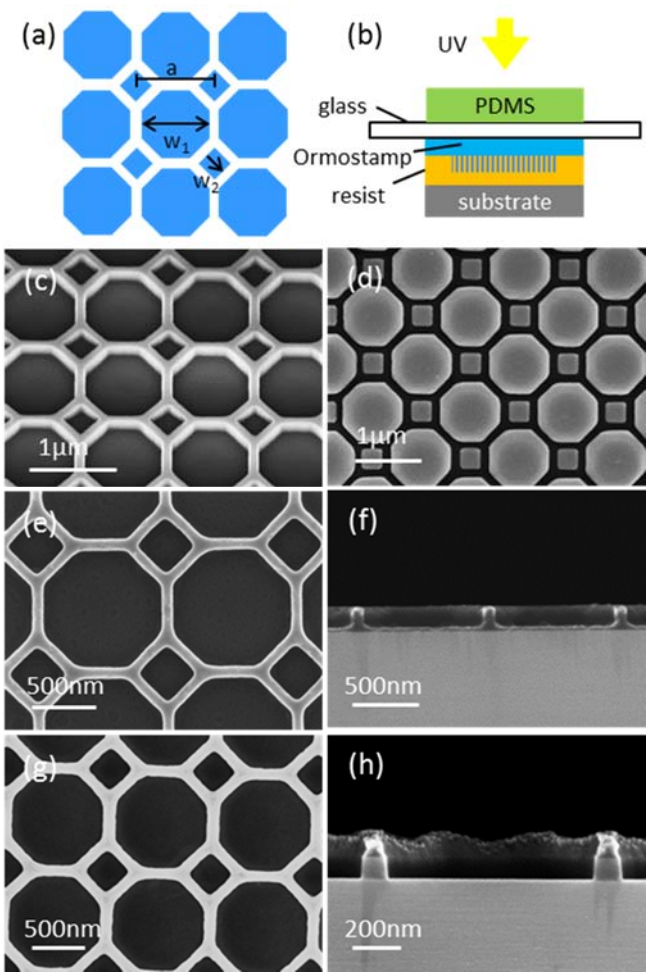

Fig. 1. (a) Layout of the superlattice PhC with period a=1 µm, octagon width w_1=0.905 µm, square side length w_2=0.34 µm. (b) Schematic view of the UV-NIL process with a flexible stamp (not to scale). (c) Scanning electron micrograph of the Si template. (d) Flexible stamp: Ormostamp on a 150 µm thin glass slide. (e,f) PhC imprinted into the resist layer, with residual resist layer. (g,h) PhC etched into the SiO_2 mask layer, with remaining resist on top. Cross-sections were taken from Si test samples.

To fabricate the stamp, the Si master was coated with an anti-sticking layer (BGL-GZ-83, Profactor GmbH) and replicated into Ormostamp® (microresist technology GmbH) on the glass substrate, which was treated with Ormoprime® as adhesion promoter. Next, the stamp surface was coated with an antisticking layer and the cleaned Ta substrates were treated with TI prime adhesion promoter (MicroChemicals). Then UV-curable resist (mr-UVCur21, microresist technology GmbH) was spin-coated onto the substrates, and the stamp imprinted into the resist and cured by UV exposure. The imprinted structures had narrow ridges of approx. 85-95 nm width between cavities of approx. 905 nm (inner diameter octagons) and 340nm (side length squares), with very steep sidewalls (see Fig. 1), which ensures the accurate transfer of the pattern into the substrate in the subsequent etching steps. The ridges were almost 200 nm high, corresponding to the Si template, with an aspect ratio of 2:1. The dense pattern and consequently high fill factor of the pattern (79.4%) caused a slight variation of the thickness of the residual resist layer over the imprinted area (circle with 3.6 mm diameter): About 30 nm of resist remaining in the center, and vanishing towards the edges of the circle. After etching of the residual resist layer in oxygen plasma, the pattern was transferred into the SiO_2 mask layer by reactive ion etching (RIE) with a selectivity of about 2:1 using 20 sccm CHF_3, 20 mTorr and 120 W. Finally, the pattern was etched into the Ta substrate by DRIE using a Bosch process with SF_6 and C_4F_8 as the etching and passivating

species, respectively.[20] The resulting cavities had very smooth and steep sidewalls, which is critical to the spectral properties, with a depth of about d=2.2 µm and an aspect ratio of more than 6:1 (see Fig. 2). The remaining SiO_2 mask was removed by diluted hydrofluoric acid (HF). In the last step, a 40nm-thick layer of HfO_2 was deposited conformally on the Ta PhC by atomic layer deposition (ALD, Cambridge Nanotech) at a substrate temperature of 130°C. The final square and octagon cavities were 260 nm and 825 nm wide, respectively, with ridges of approximately 165-175 nm width between the cavities.

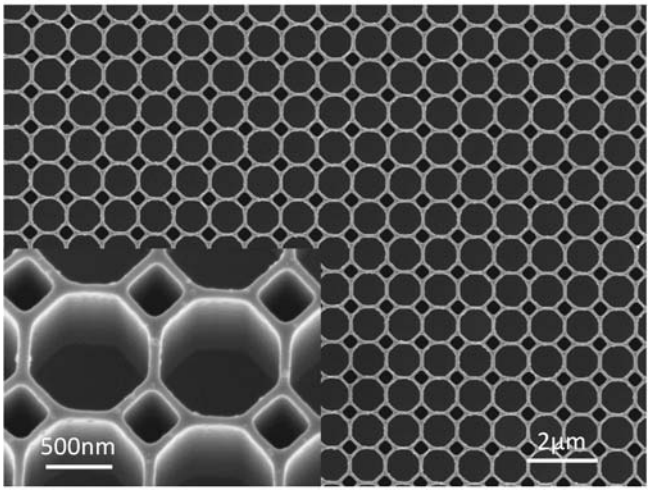

Fig. 2. Scanning electron micrograph of the fabricated superlattice PhC etched 2.2 µm deep into the Ta substrate.

The proposed superlattice PhC was designed and optimized to have broadband absorptivity approaching the blackbody limit in the visible and near-infrared (NIR) spectral range while keeping the thermal emissivity low. As a figure of merit, the thermal transfer efficiency of the absorber η_T was calculated, which denotes the difference between absorbed and thermally re-emitted power, normalized by the input power:[26]

$$\eta_T = \bar{\alpha} - \bar{\varepsilon} \cdot \frac{\sigma T^4}{H_S}, \quad (1)$$

$$\bar{\alpha} = \frac{1}{H_S} \int_0^\infty d\lambda \varepsilon(\lambda) S_S(\lambda), \quad (2)$$

$$\bar{\varepsilon} = \frac{\int_0^\infty d\lambda \varepsilon(\lambda) / \{\lambda^5 (e^{\frac{hc}{\lambda kT}} - 1)\}}{\int_0^\infty d\lambda / \{\lambda^5 (e^{\frac{hc}{\lambda kT}} - 1)\}}, \quad (3)$$

where $\bar{\alpha}$ is the solar absorptivity, $\bar{\varepsilon}$ is the thermal emissivity, and σ the Stefan-Boltzmann constant, T the operating temperature, H_S is the total solar irradiance, $S_S(\lambda)$ is the solar spectrum (AM1.5D), $\varepsilon(\lambda)$ is the spectral emittance of the absorber, λ is the wavelength of light, h is the Planck constant, c is the speed of light and k is the Boltzmann constant. The numerical simulations of the spectral properties of the PhC were performed using a rigorous coupled-wave analysis (RCWA) algorithm (S^4, Ref. 27) and verified by a finite-difference time-domain (FDTD) algorithm (MEEP, Ref. 28). The material properties of Ta as the substrate material were taken into account using the dispersion relation of Ta at high temperature, taken from the literature[29] to calculate the spectral properties of the PhC absorber at high temperature. For room temperature simulations, the dispersion of a polished Ta measured at room temperature was used. Note that the spectral absorptance and emittance is also angle-dependent, and to calculate the thermal emissivity, the hemispherical spectral emittance of the PhC was taken into account. For operating conditions of T=1500 K and H_S=1000 kW/m² incident irradiance, the optimized superlattice has a period a=1.0 µm, width w_1=0.905 µm and w_2=0.34 µm and an HfO_2 coating with thickness 40 nm. Although the solar absorptivity increases with etching depth of the cavities in Ta, $\bar{\alpha}$ is already higher than 96% for an etch depth above 2.0 µm. A further increase in etching depth was found to have only a diminishing increase in $\bar{\alpha}$. The thermal transfer efficiency is η_T=82.8% (1500 K, 1000 kW/m2) for an etching depth of 2.2 µm. The spectral absorptance and the calculated thermal emission of this superlattice PhC absorber at 1500 K are displayed in Fig. 3. Due to the contributions from cavity modes of both the square and the octagonal cavities and the additional HfO_2 coating, the spectral region of high absorptance spans approx. from 300 nm to 1900 nm, covering the range of the solar spectrum with significant irradiance. There is a steep cut-off of the absorptance (=emittance) at 1900 nm so that the calculated thermal emissivity of the PhC at 1500 K as defined in Eq. 3 is $\bar{\varepsilon}$=0.46. I.e., in comparison to a blackbody emitter the emission of the PhC is reduced by more than a factor 2. For an efficient absorber-emitter pair in STPV the area ratio of the absorber to the emitter can be reduced below 1. Then the system efficiency increases since the losses by re-emission from the absorber are minimized, albeit at an increase of the irradiance needed to achieve high operating temperatures.[2,16,18] Therefore, the area of the superlattice PhC absorber is 10mm² to achieve an area ratio of 0.1 in a 1cm x 1cm planar absorber-emitter geometry.[18]

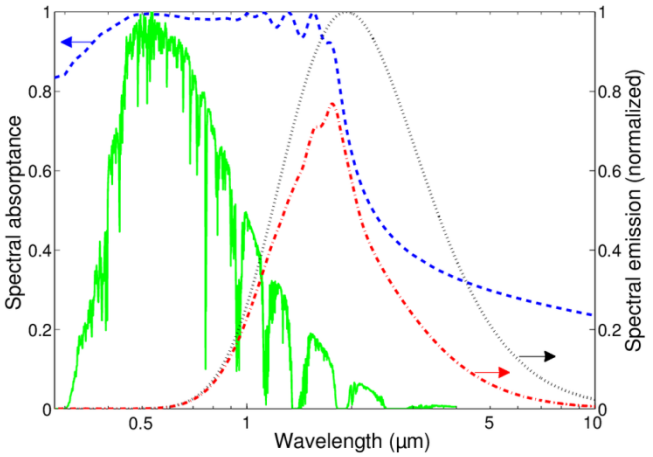

Fig. 3. Simulated spectral normal absorptance of the optimized superlattice PhC (blue, dashed line) as compared to the solar spectrum (AM1.5D, normalized, green solid line), and the spectral hemispherical emission at 1500 K of the superlattice PhC (red, dashed-dotted) compared to blackbody emission at 1500 K (black, dotted, normalized).

To characterize the spectral performance of the fabricated samples, their reflectance was measured at room temperature from 600 nm to 10 µm using an FTIR (Bruker Vertex80) with a pyroelectric (Deuterated triglycine sulfate, DTGS) detector for the infrared and a Si detector for the visible range. The incident angle of irradiance on the sample was 15° and the collection angle from the sample about 30°. In addition, a spectrophotometer with a 150 mm InGaAs integrating sphere (Perkins-Elmer Lambda 1050) was used to measure the total reflectance from 300 nm to 1400 nm, capturing also diffraction and diffuse reflection. Since the sample was opaque, the absorptance can be derived from the measured reflectance using Kirchhoff's law: A=1-R. As can be seen in Fig. 4, the measured spectrum shows excellent agreement with the simulated one (at room temperature). The absorptance approaches 1 (i.e., reflectance is close to zero) in the range from 450 nm to 900 nm, where the solar spectrum has its maximum. For wavelengths above 2µm the absorptance approaches that of flat Ta, ensuring low thermal emissivity.

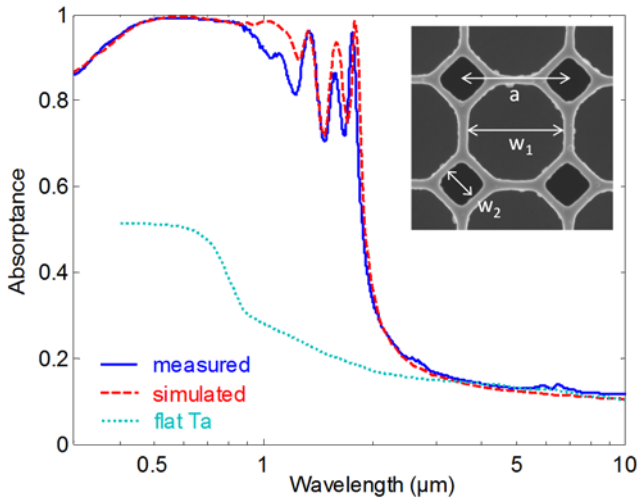

Fig. 4. Absorptance spectra derived from the reflectance measured at room temperature (blue solid line), compared to simulation (red dashed line) for a PhC with period a=1.0 μm, width w_1=0.905 μm and w_2=0.34 μm, etching depth d=2.2 μm and d(HfO_2)=40 nm; and flat Ta (light blue dotted line).

In conclusion, 2D superlattice PhC consisting of a pattern of octagonal and square cavities in a Ta substrate was designed and fabricated as a solar absorber for high temperature applications. The geometry was tailored to achieve maximum thermal transfer efficiency for operating conditions of 1500 K and an irradiance of 1000 kW/m^2, and has a period of a=1.0 μm, width w_1=0.905 μm and w_2=0.34 μm of the octagonal and square cavities, respectively. An additional HfO_2 coating of 40 nm serves both as anti-reflection and surface protection coating. The superlattice PhC was fabricated on polished Ta substrates by UV-NIL, using a flexible stamp to ensure uniform contact. Despite the high fill factor of almost 80%, the pattern was replicated with excellent uniformity and good accuracy over an area of 10mm^2. It was transferred into a SiO_2 hard mask by RIE and finally etched into Ta by DRIE using a SF_6 and C_4F_8 based Bosch process. The resulting superlattice PhC was 2.2μm deep, having ridges of 85-95nm width between the cavities and vertical sidewalls. In the last step a conformal HfO_2 coating was deposited by ALD. The spectral absorptance derived from reflectance measurements at room temperature shows high absorptance in the range from approx. 300 nm to 1900 nm with a steep drop at 1900 nm, and low absorptance approaching that of bare Ta for longer wavelengths. The experiments are in excellent agreement with numerical results, which predict a solar absorptivity of 96% at high temperature (1500 K) and a thermal transfer efficiency of 82.8% (1500 K, 1000 kW/m2) for a superlattice PhC absorber with this geometry. These results demonstrate that the superior tailoring capacity of the superlattice PhC geometry is ideal to achieve highly selective absorption and emission, which is crucial for high efficiency high temperature energy conversion. The fabrication by NIL is paving the way towards a high-throughput, high-resolution fabrication of complex high-temperature photonic components.

Funding: Austrian Science Fund (FWF) (J3161-N20); Army Research Office (W911NF-13-D-0001); Department of Energy, S3TEC Energy Research Frontier Center (DE-SC0001299).

Acknowledgements: V. R. would like to thank P. Rauter and M. Scharber for assistance with characterization, I. Bergmair for helpful discussions, and A. Halilovic for technical assistance.

REFERENCES

1. R. M. Swanson, Proceedings of the IEEE, 67, 446 (1979).
2. N-P. Harder and P. Würfel, Semicond. Sci. Technol. 18, S151 (2003).
3. E. Rephaeli and S. Fan, Opt. Express 17, 15145 (2009).
4. A. Datas and C. Algora, Prog. Photovolt: Res. Appl. 21, 1040 (2013).
5. A. Heinzel, V. Boerner, A. Gombert, B. Bläsi, V. Wittwer, and J. Luther, Journal of Modern Optics 47, 2399 (2000).
6. J. G. Fleming, S. Y. Lin, I. El-Kady, R. Biswas, and K. M. Ho, Nature 417, 52 (2002).
7. H. Sai, Y. Kanamori, and H. Yugami, Appl. Phys. Lett. 82, 1685 (2003).
8. I. Celanovic, N.Jovanovic, and J. Kassakian, Appl. Phys. Lett. 92, 193101 (2008).
9. E. Rephaeli and S. Fan, Appl. Phys. Lett.92, 211107 (2008).
10. Y. X. Yeng, M. Ghebrebrhan, P. Bermel, W. R. Chan, J. D. Joannopoulos, M. Soljačić, and I. Celanovic, PNAS 109, 2280 (2012).
11. C. Schlemmer, J. Aschaber, V. Boerner, and J. Luther, AIP Conf. Proc. 653, 164 (2003).
12. P. Nagpal, D. P. Josephson, N. R. Denny, J. DeWilde, D. J. Norris, and A. Stein, J. Mater. Chem. 21, 10836 (2011).
13. K. A. Arpin, M. D. Losego, and P. Braun, Chem. Mater. 23, 4783 (2011).
14. V. Rinnerbauer, Y. X. Yeng, W. R. Chan, J. J. Senkevich, J. D. Joannopoulos, M. Soljačić, and I. Celanovic, Opt. Express 21, 11482 (2013).
15. A. Datas and C. Algora, Prog. Photovolt: Res. Appl. 21, 1099 (2012).
16. A. Lenert, D. M. Bierman, Y. Nam, W. R. Chan, I. Celanovic, M. Soljačić, and E. N. Wang, Nat. Nano. 9, 126 (2014).
17. V. Rinnerbauer, A. Lenert, D. M. Bierman, Y. X. Yeng, W. R. Chan, R. D. Geil, J. J. Senkevich, J. D. Joannopoulos, E. N. Wang, M. Soljačić, and I. Celanovic, Adv. Energy Mater. 4, 1400334 (2014).
18. V. Rinnerbauer, Y. Shen, J. Joannopoulos, M. Soljačić, F. Schäffler, and I. Celanovic, Opt. Express 22, A1895 (2014).
19. M. Araghchini, Y. X. Yeng, N. Jovanovic, P. Bermel, L. A. Kolodziejski, M. Soljačić, I. Celanovic, and J. D. Joannopoulos, J. Vac. Sci. Technol. B 29, 061402 (2011).
20. V. Rinnerbauer, S. Ndao, Y. X. Yeng, R. D. Geil, J. J. Senkevich, K. F. Jensen, J. D. Joannopoulos, M. Soljačić, and I. Celanovic, J. Vac. Sci. Technol. B 31, 011802 (2013).
21. V. Stelmakh, V. Rinnerbauer, R. D. Geil, P. R. Aimone, J. J. Senkevich, J. D. Joannopoulos, M. Soljačić, and I. Celanovic, Appl. Phys. Lett. 103, 12, 123903 (2013).
22. S. Y. Chou, P. R. Krauss, and P. J. Renstrom, Appl. Phys. Lett. 67, 3114 (1995).
23. J. Haisma, M. Verheijen, K. van den Heuvel, and J. van den Berg, J. Vac. Sci. Technol. B 14, 4124 (1996).
24. H. Schift, J. Vac. Sci. Technol. B 26, 458 (2008).
25. I. Bergmair M. Mühlberger, M. Gusenbauer, R. Schöftner, and K. Hingerl, Microelectronic Engineering 85, 822 (2008).
26. P. Bermel, M. Ghebrebrhan, W. Chan, Y. X. Yeng, M. Araghchini, R. Hamam, C. H. Marton, K. F. Jensen, M. Soljačić, J. D. Joannopoulos, S. G. Johnson, and I. Celanovic, Opt. Express 18, A314 (2010).
27. V. Liu and S. Fan, Comput. Phys. Commun. 183, 2233 (2012).
28. A. F. Oskooi, D. Roundy, M. Ibanescu, P. Bermel, J. D. Joannopoulos, and S. G. Johnson, Comput. Phys. Commun. 181, 687 (2010). http://ab-initio.mit.edu/meep.
29. Y. S. Touloukian and D. P. DeWitt, *Thermophysical Properties of Matter*, (Plenum, New York, 1970), Vol. 7.